Research Article Vol. 16, No. 2 / 1 Feb 2025 / Biomedical Optics Express 382
Biomedical Optics EXPRESS

Feature fusion analysis approach based on synchronous EEG-fNIRS signals: application in etomidate use disorder individuals

TIANXIN GAO,[1] CHAO CHEN,[1] GUANGYAO LIANG,[1] YUCHEN RAN,[1] QIUPING HUANG,[2] ZHENJIANG LIAO,[3] BOLIN HE,[4] TEFU LIU,[4] XIAOYING TANG,[1] HONGXIAN CHEN,[3,5] AND YINGWEI FAN[1,6]

[1]*School of Medical Technology, Beijing Institute of Technology, China*
[2]*Department of Psychology, School of Humanities and Management, Hunan University of Chinese Medicine, China*
[3]*Department of Psychiatry, The Second Xiangya Hospital, Central South University, Changsha, Hunan, China*
[4]*Lituo Drug Rehabilitation Center of Hunan Province, Hunan, China*
[5]*shenhx2018@csu.edu.cn*
[6]*fanyingwei@bit.edu.cn*

Abstract: Etomidate is commonly used for induction of anesthesia, but prolonged use can affect brain neurovascular mechanisms, potentially leading to use disorders. However, limited research exists on the impact of etomidate on brain function, and accurately and noninvasively extracting and analyzing neurovascular brain features remains a challenge. This study introduces a novel feature fusion approach based on whole-brain synchronous Electroencephalography (EEG)-functional near-infrared spectroscopy (fNIRS) signals aimed at addressing the difficulty of jointly analyzing neural and hemodynamic signals and features in specific locations, which is critical for understanding neurovascular mechanism changes in etomidate use disorder individuals. To address the challenge of optimizing the accuracy of neurovascular coupling analysis, we proposed a multi-band local neurovascular coupling (MBLNVC) method. This method enhances spatial precision in NVC analysis by integrating multi-modal brain signals. We then mapped the different brain features to the Yeo 7 brain networks and constructed feature vectors based on these networks. This multilayer feature fusion approach resolves the issue of analyzing complex neural and vascular signals together in specific brain locations. Our approach revealed significant neurovascular coupling enhancement in the sensorimotor and dorsal attention networks ($p < 0.05$, FDR corrected), corresponding with different frequency bands and brain networks from single-modal features. These features of the intersection of bands and networks showed high sensitivity to etomidate using machine learning classifiers compared to other features (accuracy: support vector machine (SVM) - 82.10%, random forest (RF) - 80.50%, extreme gradient boosting (XGBoost) - 78.40%). These results showed the potential of the proposed feature fusion analysis approach in exploring changes in brain mechanisms and provided new insights into the effects of etomidate on resting neurovascular brain mechanisms.

1. Introduction

Etomidate is an imidazole-derived, ultrashort-acting, nonbarbiturate sedative commonly used during conscious sedation endoscopy or induction for an operation under general anesthesia [1]. Since it is a psychoactive substance and easy to purchase [2], there is evidence that etomidate use disorders could contribute to a global substance use crisis [3]. Substance use disorders can lead to impaired brain function [4] and have long-term effects on the neurovascular unit in the brain

#542078 https://doi.org/10.1364/BOE.542078
Journal © 2025 Received 11 Sep 2024; revised 28 Nov 2024; accepted 15 Dec 2024; published 3 Jan 2025

Biomedical Optics EXPRESS

[5]. However, there is limited research on the neurovascular brain mechanism changes caused by etomidate use disorder currently.

Being noninvasive, flexible, portable, easy to use, and capable of providing direct, real-time assessments of brain activity [6,7], electroencephalography (EEG) and functional near-infrared spectroscopy (fNIRS) provide complementary information, and the synchronous acquisition and analysis of the two signals can provide a more comprehensive understanding of neurovascular brain function [8], hence have gained popularity for studying brain function in individuals with substance use disorders. EEG records electrical activity caused by neuronal activity in the cerebral cortex, whereas fNIRS measures changes in oxyhemoglobin (HbO) and deoxyhemoglobin (HbR) concentrations. Neural activity increases local metabolic demand, triggering NVC processes that elevate cerebral blood flow (CBF). The aim of NVC is to ensure oxygen supply of neural activities. HbO is an indicator of blood oxygen supply, hence HbO signals are used to study the NVC activity as well. The reliability of this method has been proofed [9–11]. EEG's high temporal resolution and fNIRS's sensitivity to blood flow changes provide great convenience for research. On the one hand, EEG and fNIRS independently + provide insights into distinct aspects of brain function: EEG captures rapid electrical activity patterns resulting from neuronal activity, while fNIRS measures slower hemodynamic changes. On the other hand, their synchronous use allows for a comprehensive examination of the differences and connections between electrical and hemodynamic patterns underlying various brain functions. This dual-modality approach not only enables the study of neurovascular coupling with high temporal and spatial resolution but also enhances the accuracy and robustness of feature fusion methods for classification, making it particularly effective for identifying neurophysiological alterations in individuals with substance use disorders [12,13].

Synchronous acquisition and analysis of EEG-fNIRS data may reveal more comprehensive information related to brain activity. However, EEG signals are characterized by low spatial resolution, and the synchronous EEG-fNIRS signal acquisition device usually combines discrete EEG and fNIRS signal acquisition devices by assembly, bulky optical fibers, EEG cabling, and electrodes inherently compete for space on the head. This is particularly the case for devices with high-density probes. So it is difficult to synchronously collect neurovascular information at the same location [14,15], which makes it difficult to accurately measure the degree of neurovascular coupling at specific locations and integrate feature information obtained by EEG and near-infrared signals from different kinds of channels.

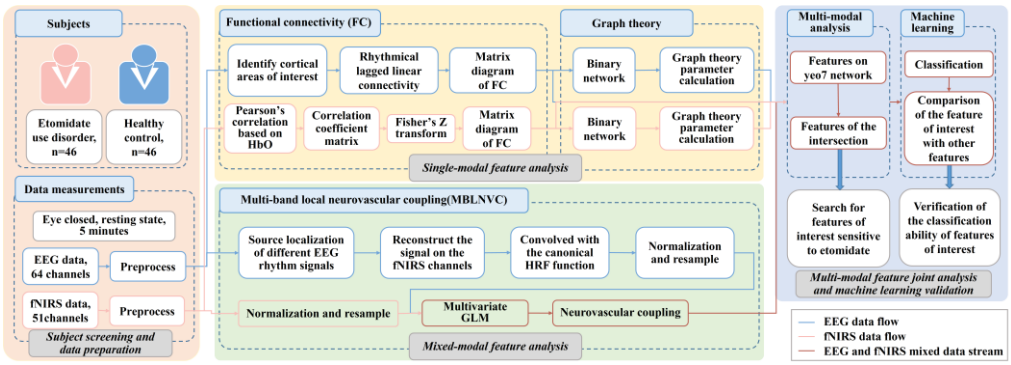

Fig. 1. Research flowchart.

Aiming at the gap of EEG-fNIRS joint analysis techniques, this study proposed a feature fusion approach based on synchronous EEG-fNIRS signals. First, single-modal signal analysis, including resting-state functional connectivity analysis and brain network graph theory analysis,

Biomedical Optics EXPRESS

was performed to explore spatial and frequency distribution differences in single-modal EEG and fNIRS features between etomidate use disorder individuals and healthy controls. Second, by locating the source of EEG signals and reconstructing them on the near-infrared channels, the multi-band local neurovascular coupling (MBLNVC) analysis method was carried out, and the physiological function changes of each position of the brain were observed from the perspective of neurovascular coupling. Furthermore, the Yeo 7 networks were used to integrate the multi-modal features of the two groups to find the Yeo 7 networks and EEG frequency sensitive to etomidate. Finally, machine learning classifiers were used to verify the ability of these sensitive features to identify etomidate use disorders. The research process is shown in Fig. 1.

2. Materials and methods

2.1. Subjects

This study included 46 individuals with etomidate use disorder and 46 healthy controls with synchronous EEG-fNIRS resting-state data. All the subjects were males aged 16–55 years who consented to participate in this study and signed informed consent forms. The exclusion criteria included intracranial hypertension; skull defects; tumor patients; severe physical diseases (e.g., cardiovascular, liver, kidney, gastrointestinal diseases); infectious diseases; immune system diseases; a history of mental illness; severe neurological diseases; and mental retardation. Etomidate use disorder individuals had used etomidate within a month before data collection without other substance use history, with substance use disorder severity of mild or above (≥ 2 symptoms on the DSM-5 scale [16]). The ETO specific sample selection procedures are shown in Appendix Fig. S1.

The demographic information and test results for the two groups are shown in Table 1. To meet the statistical sample size estimation requirements, age and education level were included as covariates in subsequent EEG and fNIRS feature comparisons to eliminate their effects on the analysis results.

Table 1. Demographic information of the subjects and test results

Group	Age (years)	Education Level (Middle School and Below / High School / Undergraduate or College)
Healthy Control	24 ± 9	5 / 34 / 7
Etomidate	22.5 ± 11.5	31 / 9 / 6
p	0.056[a]	0.000[b]

[a]Independent sample t-test.
[b]Chi-square test; $p < 0.05$ is considered statistically significant.

2.2. EEG and fNIRS measurements

2.2.1. Acquisition equipment

This study used a 64-channel EEG device (NeuSen W, Neuracle Technology Co., Ltd.). The EEG cap electrodes covered most scalp areas according to the 10-10 positioning system. The REF electrode was used as the reference electrode for all channels during EEG recording, keeping all channel electrode impedances below 5 kΩ. The sampling frequency was 1 kHz. The fNIRS signals were measured by a 51-channel near-infrared brain functional imaging system (NirSmart-6000A, Danyang Huichuang Medical Equipment Co., Ltd., China). The fNIRS device included 23 NIRS emitters and 16 detectors and used dual-wavelength NIR lasers (730 nm and 850 nm) to detect blood oxygen changes (oxyhemoglobin and deoxyhemoglobin concentration changes) at a sampling frequency of 11 Hz. The spatial coordinates of the fNIRS channels were determined based on the standard international 10-20 electrode placement system. These

Biomedical Optics EXPRESS

coordinates were then converted into Montreal Neurological Institute (MNI) space using a transformation algorithm provided by the Nirspace magnetic source navigation system (Danyang Huichuang Medical Equipment Co., Ltd., Danyang, Jiangsu, China). This system employs spatial registration methods to project the channel positions onto the MNI standard brain template, ensuring accurate localization relative to standard anatomical references. The EEG electrodes and fNIRS probes were fixed on the same probe cap for synchronous detection. The location of the detection cap channel collected by EEG-fNIRS in this experiment is shown in Fig. 2(A) (all the brain images in this paper were drawn via BrainNetViewer [17]). The synchronization error of the multi-modal signals was less than 100 ms. Experimental devices and paradigm for synchronous resting-state EEG-fNIRS recordings is shown in Fig. 2(D).

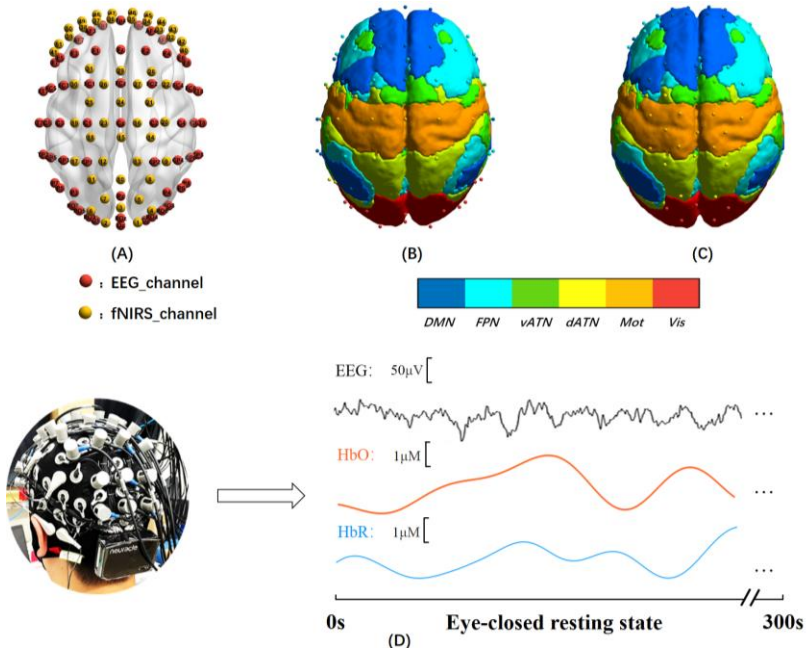

Fig. 2. (A) Schematic diagram of the channels of the joint collection detection cap. (B) EEG channels and their corresponding Yeo 7 networks. (C) fNIRS channels and their corresponding Yeo 7 networks. (D) Experimental devices and paradigm for synchronous resting-state EEG-fNIRS recordings.

2.2.2. Acquisition procedures

The signal acquisition for this experiment was conducted in a dedicated collection room (etomidate use disorder individuals (ETO): Hunan Province Lituo Compulsory Isolation Drug Rehabilitation Center, healthy controls (HC): Beijing Institute of Technology), with only the subject and the main experimenter present. During the experiment, the subjects sat still while their EEG-fNIRS signals were collected in a closed-eye state for 5 minutes. No specific task or stimuli were presented during the experiment. The study was approved by the Ethics Committee of the National Clinical Medical Research Center of the Second Xiangya Hospital of Central South University (No. 2023K003).

2.2.3. Data preprocessing

The EEG data were first downsampled to 250 Hz, and unnecessary channels (five ECG and EOG channels not connected during acquisition) were removed. The remaining 59 channels

Biomedical Optics EXPRESS

were re-referenced by the whole brain. The data were then bandpass filtered from 1-40 Hz and notch-filtered at 50 Hz (using Basic FIR filters). Next, independent component analysis (ICA) was performed to obtain 59 independent components for each subject, manually removing potential eye movement and muscle contraction artifacts, resulting in clean EEG data. Finally, the data were filtered (via basic FIR filters) to obtain signals in five rhythms: δ (1-3 Hz), θ (3-8 Hz), α (8-13 Hz), β (13-30 Hz), and γ (30-40 Hz). These EEG preprocessing steps were completed via the open-source toolkit EEGLAB, which is based on MATLAB software [18].

For fNIRS data, the light signals from the fNIRS acquisition system were first converted to changes in oxyhemoglobin and deoxyhemoglobin concentrations via the modified Beer-Lambert law [19]. A polynomial regression model was then used to estimate linear or nonlinear trends, which were regressed from the original hemoglobin concentration signals. Then, motion artifacts were corrected via the TDDR method [20]. Finally, IIR filter is used to filter the signals at 0.01-0.2 Hz. HbO signals were chosen as the primary indicator for analyzing hemodynamic responses because they exhibit greater sensitivity to neural activity-induced changes and larger amplitude variations compared to HbR signals, resulting in a higher signal-to-noise ratio [21]. These fNIRS preprocessing steps were completed via the open-source toolkit NIRS_KIT via MATLAB software [22].

2.3. Single-model feature analysis

2.3.1. Functional connectivity analysis

The EEG signal is characterized by low spatial resolution and volume conduction effects. To address these issues, we used the sLORETA tool [23] to define 59 regions of interest (ROIs) corresponding to the EEG channels. We selected the single voxel closest to each channel as the ROI. The functional connectivity strength between ROIs was then evaluated by calculating lagged linear correlations. Before calculating the functional connectivity strength, we segmented the data of each ROI into 10-second intervals, calculated the functional connectivity strength for each segment, and averaged the results of all segments.

The functional connectivity measurements provided by sLORETA decompose connectivity into instantaneous and lagged components. The instantaneous component is largely contaminated by the volume conduction effect of the EEG signal, where the zero-lag spread of the electric field from its source to the tissue leads to nonphysiological inflation of the instantaneous connectivity measurement. Removing the instantaneous zero-lag component can effectively eliminate the volume conduction effect, resulting in a true linear correlation (lagged coherence) matrix between cortical source activities [24]. This matrix is used for subsequent brain connectivity and brain network analysis.

For fNIRS signals, we calculated the correlation coefficient matrix between the 51 channels in the time series via Pearson correlation analysis. Fisher's Z-transformation was then applied to the matrix for nonlinear correction to ensure a normal distribution, obtaining a functional connectivity matrix for subsequent analysis.

2.3.2. Graph theory analysis

We used graph theory analysis to understand the changes in the functional nodes and the attributes of the entire brain network at specific locations. This analysis was performed by constructing binary networks from the functional connectivity matrices derived from EEG and fNIRS time-domain information, allowing us to calculate various network attributes.

In these networks, the nodes correspond to the ROIs in EEG or channels in fNIRS. A threshold was applied to determine an equal number of edges for network construction to ensure comparability between groups. Since there is no consensus on the optimal threshold, we employed a broad range of thresholds ($0.05 \leq T \leq 0.5$, with increments of 0.05) to construct the network

Biomedical Optics EXPRESS

edges. We used the AUC (area under the curve) values corresponding to these thresholds as a stable feature estimation.

In this study, we focused on ten graph theory metrics: nodal betweenness centrality, nodal degree centrality, the nodal clustering coefficient, nodal efficiency, nodal local efficiency, global efficiency, local efficiency, the clustering coefficient, the characteristic path length, and small-world properties. Detailed definitions and explanations of these metrics can be found in Appendix Table S1. The calculation of brain network parameters was performed via the open-source toolbox Gretna, which is based on MATLAB software [25].

2.4. Mixed-modal feature analysis

With the neural activity acquired with EEG technique and the hemodynamic response acquired with fNIRS technique, we proposed a MBLNVC analysis method to perform feature fusion of the data layers. The calculation of MBLNVC via EEG-fNIRS involves two main steps. The first step involves further processing the preprocessed EEG and fNIRS signals to standardize them into comparable time series data. The second step is determining the degree of coupling between the two results.

For the EEG data, we used the sLORETA tool to perform source localization on the five frequency bands of the preprocessed EEG signals. This provided the current source density for each EEG rhythm in cortical voxels. We then defined 51 ROIs corresponding to the positions of the fNIRS channels: each channel was associated with the nearest voxel as its ROI, yielding the current source density for each ROI. The current source densities of the five EEG components were normalized (z-score). We subsequently convolved the time series data of each ROI with the standard hemodynamic response function (HRF) to obtain the expected changes in the hemoglobin concentration. The standard HRF function is composed of two gamma functions:

$$HRF(t) = \frac{b_1^{a_1} * t^{(a_1-1)}}{\Gamma(a_1)} * e^{(-b_1 * t)} - c * \frac{b_2^{a_2} * t^{(a_2-1)}}{\Gamma(a_2)} * e^{(-b_2 * t)} \tag{1}$$

where t represents time points, a_1 and a_2 are the time delays of the positive and negative peaks, b_1 and b_2 are the dispersion time constants of the positive and negative peaks, c is the amplitude ratio of the positive to negative peaks, and Γ is the gamma function. The specific parameters were set to the default parameters of NIRS_SPM ($b_1, b_2 = 1$, $a_1 = 6$, $a_2 = 16$, $c = 1/6$) [26].

Finally, we normalized (z-score) and resampled (1 Hz) the expected hemoglobin concentration changes, using the resulting data as the independent variable (X_i) for input into the general linear model (GLM). The actual changes in hemoglobin concentration (HbO) were also normalized (z-score) and resampled (1 Hz), aligned in amplitude and length with the processed EEG results, and used as the dependent variable (Y) in the GLM.

We evaluated the degree of NVC for each fNIRS channel via the GLM to assess the impact of the five EEG rhythms on hemodynamics [27,28]. The form of the GLM is as follows:

$$Y = \beta_0 + \beta_1[X_1, X_2, X_3, X_4, X_5] + \epsilon \tag{2}$$

where β_0 is the intercept, β_1 is the slope, and ϵ is the error term. In our study, the processed fNIRS signals served as the dependent variable Y, whereas the processed signals of the five EEG rhythms corresponded to the independent variables $[X_1, X_2, X_3, X_4, X_5]$. through the GLM, we obtained the estimated standardized slope vector $\hat{\beta}_1$ for each fNIRS channel, reflecting the influence of each independent variable X_i on the dependent variable Y. [11]

At last, we evaluated the relationship between the standardized β values and DSM-5 scores among individuals with etomidate use disorder using Spearman's rank correlations. False Discovery Rate (FDR) correction was used to adjust the results of multiple hypothesis tests.

Biomedical Optics EXPRESS

2.5. Multi-modal feature joint analysis

We observed significant differences in age and years of education between the two groups (HC and ETO). To account for potential confounding effects, we performed covariate regression analyses on the three types of features (functional connectivity matrices calculated from EEG and fNIRS, brain network features calculated from EEG and fNIRS, and standardized β values of MBLNVC calculated from EEG-fNIRS). The correlation results showed no significant associations between these features and demographic variables (age and years of education), indicating that the extracted features are independent of these factors and primarily reflect differences in neurophysiological characteristics between the two groups. We then conducted the independent samples t-test to obtain features with significant differences. The Benjamini and Hochberg method in False Discovery Rate (FDR) correction was used to adjust the results of multiple hypothesis tests.

Each EEG and near-infrared node's MNI coordinates were mapped onto the Yeo 7 brain networks [29](The Yeo 7 brain networks include the default mode network (DMN), frontoparietal network (FPN), ventral attention network (vATN), dorsal attention network (dATN), somatomotor network (Mot), and visual network (Vis)), to find the frequency band and location of the intersection of the significantly multi-modal features and then determine the brain networks and EEG frequency band sensitive to etomidate. The correspondence between the EEG/near-infrared channels and networks is shown in Fig. 2(B) and Fig. 2(C), and the detailed channel MNI coordinates, and networks correspondence are listed in Appendix Tables S2 and S3.

2.6. Machine learning

We first ranked the significant features ($p < 0.05$, FDR corrected) via the Fisher score method, which evaluates features based on the principle that features with small within-class distances and large between-class distances are considered discriminative features [30].

According to the Fisher score results, we sorted the significant features and categorized those with location-frequency clustering features as features of interest (FOIs) and others as features of no interest (FONs). We then compared the classification performance of the FOIs, FONs, and features of all (FOAs). To ensure comparability, we selected the top 30 features from each group based on the Fisher score.

We used three classification models: SVM, RF, and XGBoost. The classification results were evaluated via five machine learning classification metrics: accuracy, precision, recall, the F1 score, and the receiver operating characteristic (ROC) curve, as shown in Appendix Table S4. At last, the stability metrics were obtained by 10-fold cross-validation.

3. Results

3.1. Functional connectivity analysis

In the analysis of brain functional connectivity, only some channels in the δ rhythm of the EEG frequency band showed significant functional connectivity after FDR correction ($p < 0.01$). Similarly, some channels in the fNIRS signals also passed FDR correction. We retained channels with significant differences and used interpolation methods to map these differences onto the cortex, using colors to indicate the degree of difference.

As shown in Fig. 3(A), the distribution of channels with significant changes in δ-band EEG connectivity was dispersed across the frontal, parietal, and occipital lobes, with more pronounced and dense changes near the central sulcus and occipital lobe. There was also clear lateralization, with more dense and intense changes in the right hemisphere. All of these parameters were significantly reduced in the etomidate group. Figure 3(B) shows that the fNIRS channel connectivity changes were more concentrated in the frontal region, all of which were significantly reduced in the etomidate group. The specific different channels are listed in Appendix Tables S5 and S6.

Biomedical Optics EXPRESS

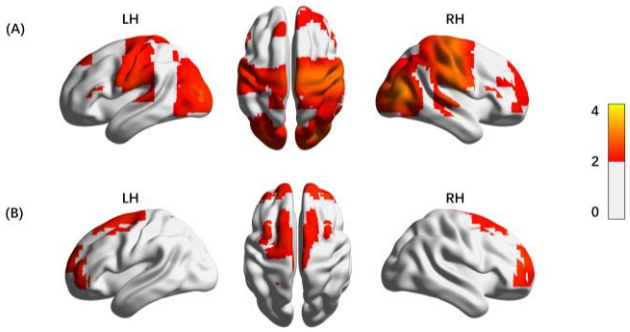

Fig. 3. (A) Locations and degrees of change on δ-band EEG channel connectivity (-log10 *p*) (with FDR-corrected *p* values). (B) Locations and degrees of change on fNIRS channel connectivity (-log10 *p*) (with FDR-corrected *p* values).

3.2. Graph theory analysis

In the brain network graph theory analysis, the significance threshold was set at $p = 0.05$ (with node graph theory features corrected by FDR). Significant differences were found only in the global graph theory features of the low-frequency bands (δ and θ) in EEG. No significant differences were found in the other EEG frequency bands or the node graph theory features across all frequency bands. Similarly, no significant differences were found in the global and node network features of the fNIRS signals.

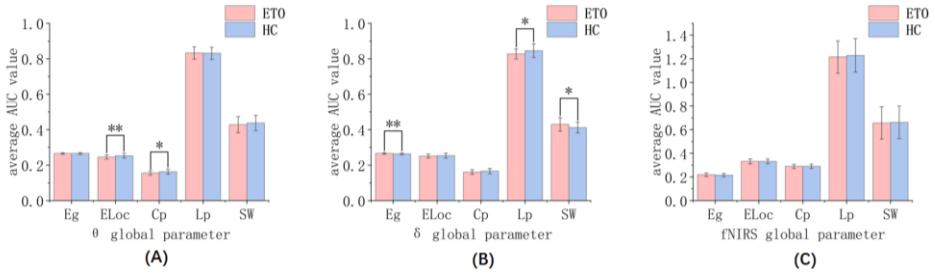

Fig. 4. (A) Comparison of the global network parameters of δ-band EEG signals between two types of people (* t-test, $0.01 < p < 0.05$; ** $p < 0.01$). (B) Comparison of the global network parameters of the θ EEG signals between the two groups of people (* t-test, $0.01 < p < 0.05$; ** $p < 0.01$). (C) Comparison of the global network parameters of fNIRS signals between two types of people.

As shown in Fig. 4. (A) In the δ band, the global efficiency of the brain network in the etomidate group was significantly enhanced ($p = 0.0097$, ETO_mean = 0.2661, HC_mean = 0.2635), the characteristic path length was significantly reduced ($p = 0.0103$, ETO_mean = 0.8272, HC_mean = 0.8454), and the small-world property was significantly enhanced ($p = 0.0147$, ETO_mean = 0.4297, HC_mean = 0.4119). As shown in Fig. 4. (B) In the θ band, the local efficiency of the brain network was significantly reduced ($p = 0.004$, ETO_mean = 0.2455, HC_mean = 0.2530), and the clustering coefficient was significantly reduced ($p = 0.0112$, ETO_mean = 0.1558, HC_mean = 0.1628). As shown in Fig. 4. (C) No significant differences were found in the global network parameters of fNIRS signals between the two groups.

Biomedical Optics EXPRESS

3.3. MBLNVC analysis

We conducted a statistical averaging of the degree of NVC for both groups. The degree of coupling was interpolated and mapped onto the cortex, with colors indicating the direction and magnitude of the mean coupling. As illustrated in Fig. 5, the differences in coupling between ETO and HC were primarily concentrated on the coupling of low-frequency EEG and hemodynamic signals, mainly in the parietal regions.

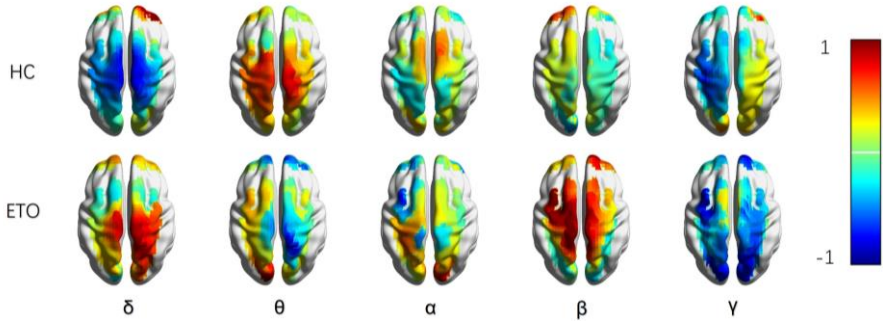

Fig. 5. Mean coupling results between fNIRS signals and the current source densities of different EEG rhythms in the two groups. Red indicates positive coupling, whereas blue indicates negative coupling.

In the coupling of δ-band EEG and hemodynamic signals, HC exhibited significant negative coupling predominantly in the parietal areas, whereas etomidate subjects showed strong positive coupling in the right parietal regions, including the precentral gyrus (BA4, 6), postcentral gyrus (BA2, 3), and parietal areas (BA7).

For the θ-band coupling, while HC displayed positive coupling in the precentral and postcentral gyri, ETO showed weak or negative coupling in the right parietal regions. The α-band coupling, HC and ETO demonstrated weak coupling with slightly difference, while in the β-band coupling, HC showed weak coupling with ETO showing positive coupling, in the precentral gyrus (BA4, 6), and dorsolateral prefrontal cortex (BA46). Finally, for the γ-band coupling, HC showed negative coupling in the left hemisphere regions and weak positive coupling in the right hemisphere with ETO showing negative coupling in the most brain regions.

We performed a t-test on the NVC results between the current source densities of the five EEG rhythms and the hemodynamic signals (HbO) for both groups, followed by FDR correction. The locations with significant coupling, as determined by FDR correction, were interpolated and mapped onto the cortex. As shown in Fig. 6. (A), significant changes in NVC were observed in certain regions for etomidate subjects. These changes were regionally clustered and frequency specific: significant differences in coupling between the two groups were observed only in the δ-band EEG and hemodynamic signals, specifically in the precentral gyrus (BA4, 6) (#13: $p = 0.0155$, ETO_mean = 0.9514, HC_mean = –0.8026; #14: $p = 0.0155$, ETO_mean = 0.8515, HC_mean = –0.7008; #15: $p = 0.0155$, ETO_mean = 0.9631, HC_mean = –0.8169; #16: $p = 0.0285$, ETO_mean = 0.7019, HC_mean = –0.7067; #20: $p = 0.0428$, ETO_mean = 0.6676, HC_mean = –0.5386; #23: $p = 0.0285$, ETO_mean = 0.7441, HC_mean = –0.6580), postcentral gyrus (BA2) (#9: $p = 0.0434$, ETO_mean = 0.7157, HC_mean = –0.5430), and parietal area (BA7) (#8: $p = 0.0224$, ETO_mean = 1.0271, HC_mean = –0.6709). The functional brain areas covered were the primary motor cortex, premotor and supplementary motor areas, somatosensory cortex, and somatosensory association cortex, which mainly involve the Mot and dATN. Significant changes were observed only in the coupling of δ-band EEG and hemodynamic signals, with etomidate subjects showing significantly enhanced positive coupling. As depicted in Fig. 6. (B), the etomidate group exhibited significantly stronger coupling than

Biomedical Optics EXPRESS

the HC group did, with positive coupling in the etomidate group and negative coupling in the HC group. The correlation test results between neurovascular coupling at the eight significantly changed frequency-band locations and ETO's DSM-5 scores were shown in Fig. 6(C), with no significant correlations observed.

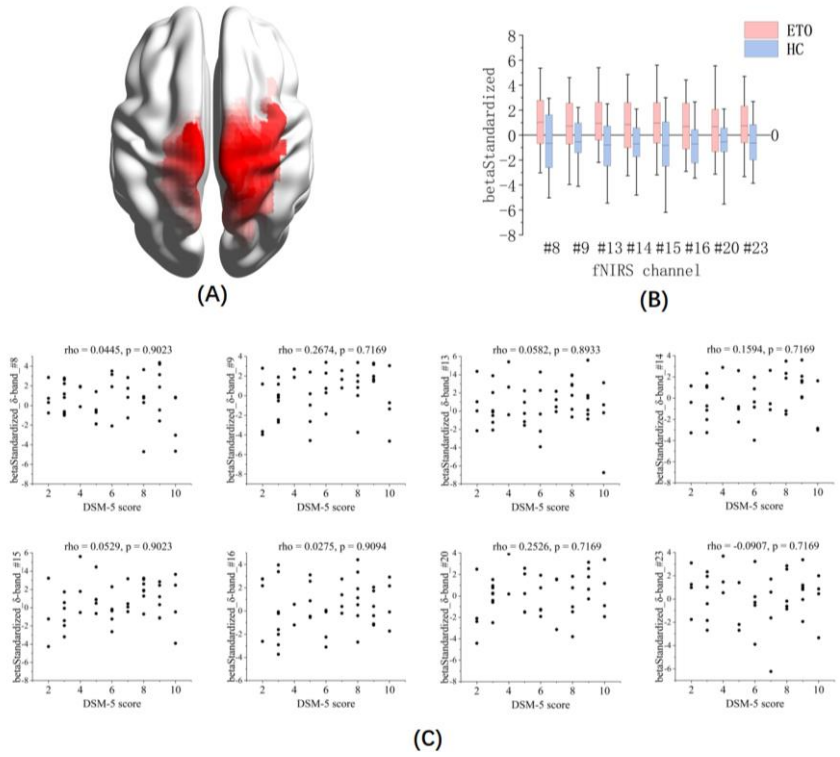

Fig. 6. (A) Locations with significant differences ($p < 0.05$, FDR corrected) in the coupling of δ-band EEG and hemodynamic signals between the two groups. Red areas indicate significantly enhanced coupling in etomidate subjects. (B) Specific channels showing significant differences in the coupling of δ-band EEG and hemodynamic signals ($p < 0.05$, FDR corrected), comparing the coupling degrees between the two groups. (C) The correlation test results between neurovascular coupling at the eight significantly changed frequency-band locations and ETO's DSM-5 scores.

3.4. Multi-modal feature joint analysis

We mapped the Mot and dATN along with the feature locations exhibiting significant changes onto a brain diagram. We also plotted the channel features within these networks, and the global graph theory feature comparisons of EEG were plotted. In the δ-band EEG and regions (Mot and dATN) where significant changes in neurovascular coupling were observed, we found that unimodal EEG features also showed more pronounced changes in these frequency bands and corresponding regions than in other frequency bands and regions.

Figure 7. (A) shows that significant differences in coupling are concentrated in the δ-band EEG and the locations of the Mot and dATN. In this frequency band and region, nearly half of the channels in the etomidate group exhibited significantly enhanced coupling. Figure 7. (B) shows that in the δ-band EEG frequency band and the corresponding EEG channels of the Mot and dATN, more than half of the channels displayed significant changes in functional connectivity. Figure 7. (C) shows that fewer relative channels with significant changes in

Biomedical Optics EXPRESS

functional connectivity in the near-infrared channels corresponding to the Mot and dATN are shown. Figure 7. (G)(H)(I) indicate that the parameters Eg, Lp, and SW all exhibited significant changes only in the δ-band EEG frequency band. In this band, the etomidate group presented significant increases in Eg, significant decreases in Lp, and significant increases in SW.

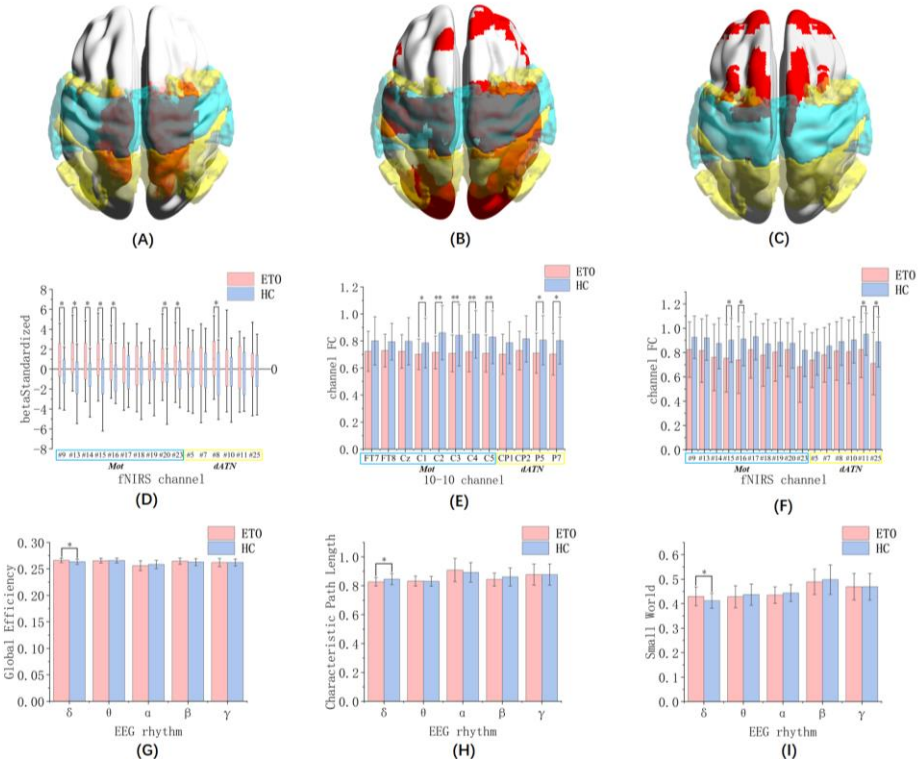

Fig. 7. (A) Locations with significant changes in neurovascular coupling (red: $p < 0.05$, FDR corrected) and their overlap with the Mot (light blue) and dATN (yellow). (B) Locations with significant changes on δ-band EEG channel connectivity and their overlap with the Mot and dATN (red: $p < 0.01$, FDR corrected). (C) Locations with significant changes in neurovascular coupling and their overlap with the Mot and dATN (red: $p < 0.01$, FDR corrected). (D) Comparison of coupling degrees on the channels of the Mot and dATN (*: $p < 0.05$, FDR corrected). (E) Comparison of δ-band EEG channel connectivity on the channels of the Mot and dATN (*: $p < 0.01$, **: $p < 0.005$, FDR corrected). (F) Comparison of fNIRS channel connectivity on the channels of the Mot and dATN (*: $p < 0.01$, **: $p < 0.005$, FDR corrected). (G) Comparison of the global graph theory parameters Eg across different EEG frequency bands between the two groups (*: $p < 0.05$). (H) Comparison of the global graph theory parameters Lp across different EEG frequency bands between the two groups (*: $p < 0.05$). (I) Comparison of the global graph theory parameter SW across different EEG frequency bands between the two groups (*: $p < 0.05$).

3.5. Machine learning analysis

We classified the ETO and HC using three sets of features: FOIs (the EEG connectivity features are δ-band EEG brain connectivity with at least one node in the intersection region, and the fNIRS connectivity features are at least one node in the intersection region), FONs, and FOAs and evaluated the classification performance using three machine learning classifiers: SVM, RF, and XGBoost. The results of 10-fold cross-validation for the three classifiers are presented

Biomedical Optics EXPRESS

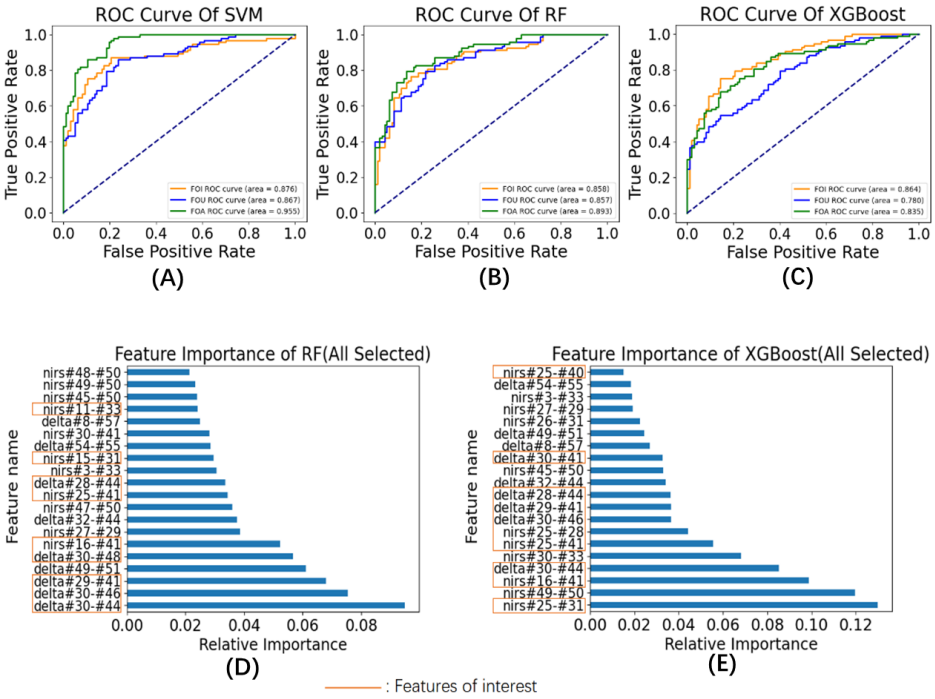

Fig. 8. (A)(B)(C) 10-fold cross-validation ROC curves and AUCs for the three feature sets across the three classifiers. (D)(E) RF and XGBoost classifiers rank the importance of all the salient features.

in Table 2. Except for the precision metric of the SVM, the FOIs consistently outperformed the FONs across all the classifiers. Compared with the FOAs, the FOIs demonstrated superior performance in the XGBoost classifier, with the accuracy improving from 76.30% to 78.40%, the precision from 76.30% to 77.30%, the recall from 75.60% to 77.00%, the F1 score from 0.75 to 0.766, and the AUC from 0.835 to 0.864. These results highlight the high efficiency of the FOIs in distinguishing between ETO and HC. As shown in Fig. 8. (D)(E), the classification importance of the FOIs is generally greater than that of the FONs, particularly among the most influential features for classification.

Table 2. Comparison of classification metrics for different models and feature sets

	SVM			RF			XGBoost		
	FOIs	FONs	FOAs	FOIs	FONs	FOAs	FOIs	FONs	FOAs
Accuracy	82.10%	77.90%	86.30%	80.50%	76.30%	81.60%	78.40%	67.40%	76.30%
Precision	79.40%	81.80%	92.20%	83.60%	78.60%	85.40%	77.30%	69.60%	76.30%
Recall	83.80%	71.60%	79.70%	76.20%	72.90%	76.90%	77.00%	60.80%	75.60%
F1_score	0.814	0.749	0.848	0.789	0.740	0.795	0.766	0.633	0.750
AUC	0.876	0.867	0.955	0.858	0.857	0.893	0.864	0.780	0.835

4. Discussions

In this study, we proposed a feature fusion approach based on synchronous resting-state EEG-fNIRS signals to address the challenge of jointly analyzing neural and hemodynamic signals

Biomedical Optics EXPRESS

at specific locations. This approach integrates neural and hemodynamic signals and features. At the data level, we introduced a MBLNVC analysis method. This method used EEG source localization techniques to obtain the current source density of EEG signals across different frequency bands on cortical voxels. The current source density was then reconstructed onto the fNIRS channels, and a multivariate GLM was applied to estimate the extent to which electrical signals influence hemodynamic signals at specific locations. This approach minimized the spatial conduction effects of EEG signals while achieving spatial alignment between neural and hemodynamic signals, enabling accurate estimation of neurovascular coupling despite the placement constraints of synchronous EEG-fNIRS devices. At the feature level, we mapped the EEG and fNIRS channel positions onto the Yeo 7 brain networks to integrate multi-modal features spatially, aiming to identify location-based correlations between different modal features.

There has been limited research on the impact of substance use disorders on neurovascular coupling mechanisms. A study on cocaine revealed that acute cocaine reduces cerebral blood flow but does not affect neuronal responses to stimuli while preserving resting-state sneurovascular coupling [31]. Our study, using portable devices and the MBLNVC analysis method, fills the gap in research on neurovascular coupling in etomidate use disorder individuals. Compared to healthy controls, we found significantly greater neurovascular coupling in the δ-band EEG within the Mot and dATN.

Mot is primarily responsible for the coordination of sensory and motor functions. We observed that in the etomidate group, during a month-long withdrawal period, the coupling between δ rhythm EEG signals and fNIRS signals in Mot was significantly enhanced. This indicates that etomidate use disorder may cause neuronal activity damage in Mot, and during withdrawal, the enhanced neurovascular coupling may be a compensatory mechanism by the brain to support the recovery of damaged neural functions by increasing blood flow. This compensatory mechanism helps meet the metabolic demands of neurons, promoting their repair and regeneration. Similar compensatory neurovascular coupling has been suggested in the context of cognitive recovery following minor strokes, where slower EEG alpha rhythms and altered synchronization might reflect compensatory processes aimed at restoring brain function after injury [32]. Furthermore, the enhanced coupling may reflect functional reorganization in Mot, particularly during the withdrawal process, where the brain may readjust neural networks to restore normal sensory and motor functions. By enhancing the coupling between δ rhythm activity and hemodynamics, Mot may more effectively coordinate sensory and motor processes.

dATN plays a crucial role in orienting and maintaining attention. During the month-long withdrawal period of individuals with etomidate, the coupling between δ rhythm EEG signals and fNIRS signals in dATN was significantly enhanced. This indicates that etomidate may cause damage to attention functions, and the brain needs to increase blood flow support to dATN during withdrawal to restore and maintain normal attention functions. The enhanced coupling may reflect the brain's heightened regulation of attention demands during withdrawal. Similarly, changes in regional cerebral blood flow during slow-wave sleep, particularly in relation to δ rhythms, highlight how neural mechanisms adapt to sensory and attention-related demands [33]. The enhanced coupling in dATN may thus be an adjustment of neural networks by the brain during the adaptation to withdrawal, ensuring the continuous and stable processing of attention-related tasks by strengthening the coupling between δ rhythm and hemodynamics. In addition to the neurovascular coupling features obtained by MBLNVC analysis, we also explored the effects of etomidate on the single-modal brain features of neural and hemodynamic signals.

For electrophysiological signals, we found a significant weakening of δ rhythm brain connectivity in individuals with etomidate use, particularly near the central sulcus and occipital lobe, mainly in the right hemisphere. This reduction may reflect etomidate's inhibitory effect on neuronal synchronization in regions associated with cognitive functions like motor control, sensory integration, visual processing, and attention. Similar findings in propofol (a similar

Biomedical Optics EXPRESS

anesthetic) studies have shown reduced sensorimotor cortex connectivity and δ connectivity after loss of consciousness [34,35]. Our research suggests that long-term etomidate-like anesthetics use may have persistent effects on brain function, with δ rhythm brain connectivity weakening potentially serving as an electrophysiological marker for this impact. For fNIRS signals, we observed that the weakening of brain connectivity was mainly concentrated in the frontal lobe. Previous studies have shown that addictive substances such as cocaine [36] and heroin [37] can lead to weakened functional connectivity in the frontal lobe, which is consistent with our results and possibly reflects the detrimental effects of substance use disorders on cognitive control functions.

On the graph theory analysis results, consistent with previous research on the effects of substance use disorders on δ-band EEG [38], we found that in δ-band EEG network analysis, global efficiency was enhanced, characteristic path length was shortened, and small-world properties were strengthened. These changes suggest improved information transmission and network coordination, potentially supporting functional stability during withdrawal. In the θ brain network, local efficiency was enhanced, and the clustering coefficient was reduced, indicating a shift toward broader network cooperation and reduced reliance on local interactions for information processing.

Our multi-modal feature analysis results indicated that the networks and EEG frequency bands exhibiting significant coupling differences in individuals with etomidate highly coincided with regions and frequency bands showing significant single-modal EEG feature changes. This coincidence indicates similar patterns of changes in these specific networks and frequency bands in individuals with etomidate use disorder, not only at the level of neural activity but also in neurovascular coupling.

After feature extraction and analysis, we identified brain networks and EEG frequency bands sensitive to etomidate by integrating multi-modal features. We employed various machine learning classifiers (SVM, RF, XGBoost) to classify individuals with etomidate and HC, evaluating the ability of these features to distinguish between the two groups. The classification results showed that features in the sensitive networks and EEG frequency bands generally outperformed other features in classification capability, achieving the best performance in the XGBoost classifier, despite they were derived from only a few brain networks and EEG frequency bands. The enhanced performance of sensitive features in the XGBoost model underscored their effectiveness in capturing the critical aspects of the data, reducing noise, and optimizing feature interactions, ultimately leading to more accurate and reliable classification outcomes. These results reveal the key impact of etomidate on these networks and EEG frequency bands and also validate the ability of the feature fusion analysis method in this study to accurately find sensitive features.

In this study, the data collected and analyzed were all from male subjects, because the proportion of women with substance use disorder was small [39]. At present, the compulsory drug rehabilitation center for scientific research cooperation is a male treatment center, and female patients with etomidate use disorder cannot be obtained. Follow-up studies will also expand cooperation units, increase the number of female etomidate use disorders, and improve the research. Additionally, HbO signals measured by fNIRS were used as a surrogate for changes in hemodynamics to explore the properties of neurovascular coupling. Although the HbO signal is essentially a partial reflection of hemodynamics, this study shows the validity of this method. The EEG-fNIRS detection is non-invasive and easy to achieve, providing a more comprehensive understanding of neurovascular coupling.

5. Conclusions

We proposed a feature fusion approach based on synchronous EEG-fNIRS signals applied in etomidate use disorder individuals. At the data layer feature fusion, we proposed a MBLNVC analysis method to measure the degree of multi-band neurovascular coupling on each near-infrared

Biomedical Optics EXPRESS

channel. Significant enhancement of the coupling between δ-band EEG and hemodynamic signals was observed in somatomotor and dorsal attention networks in the etomidate use disorder group. Besides, we found that etomidate weakens the functional connectivity of δ-band EEG signals and fNIRS signals in the resting state and alters the graph theory parameters of δ-band EEG and θ-band EEG networks. At the feature layer feature fusion, we used Yeo 7 networks partitioning to integrate multi-modal neurovascular features, and we found somatomotor and dorsal attention networks, and δ EEG band sensitive to etomidate. Then we verified features in these sensitive networks and EEG frequency bands as efficient biomarkers for judging etomidate use disorder individuals with machine learning classifiers. These results show that we found the effect of etomidate use on neurovascular brain mechanisms, and the proposed approach supports more comprehensive and detailed decoding of EEG and fNIRS signals and provides new insights for multi-modal brain feature fusion.

Funding. Science and Technology Innovation 2030 "Brain science and brain-like research" Major Project of China (2021ZD0202102); National Natural Science Foundation of China ((U20A20388)); BIT Research and Innovation Promoting Project ((Grant NO.2023YCXY044)).

Disclosures. The authors declare no conflicts of interest.

Data availability. The data that support the findings of this study are available from the corresponding author upon reasonable request.

Reference

1. DrugBank, "Etomidate (DB00292)," https://go.drugbank.com/drugs/DB00292 (accessed November 27, 2024).
2. C. Wang and N. Lassi, "Incentivizing narcotics control through China's Belt and Road Initiative in South and Southeast Asia," Journal of Developing Societies **39**(3), 259–288 (2023).
3. J. Uhm, S. Hong, and E. Han, "The need to monitor emerging issues in etomidate usage: the misuse or abuse potential," Forensic Sci., Med., Pathol. **20**(1), 249–260 (2024).
4. Y. Tian, D. Wang, F. Fan, *et al.*, "Differences in cognitive deficits in patients with methamphetamine and heroin use disorder compared with healthy controls in a Chinese Han population," Prog. Neuro-Psychopharmacol. Biol. Psychiatry **117**, 110543 (2022).
5. R. D. Egleton and T. Abbruscato, "Drug abuse and the neurovascular unit," in *Advances in Pharmacology* (Elsevier, 2014), pp. 451–480.
6. X. Gu, B. Yang, S. Gao, *et al.*, "Prefrontal fNIRS-based clinical data analysis of brain functions in individuals abusing different types of drugs," J. Biomed. Semant. **12**(1), 21 (2021).
7. F. Colledge, S. Ludyga, M. Mücke, *et al.*, "The effects of an acute bout of exercise on neural activity in alcohol and cocaine craving: study protocol for a randomised controlled trial," Trials **19**(1), 713 (2018).
8. R. Li, D. Yang, F. Fang, *et al.*, "Concurrent fNIRS and EEG for Brain Function Investigation: A Systematic, Methodology-Focused Review," Sensors **22**, 5865 (2022).
9. R. B. Govindan, A. Massaro, T. Chang, *et al.*, "A novel technique for quantitative bedside monitoring of neurovascular coupling," J. Neurosci. Methods **259**, 135–142 (2016).
10. L. F. Chalak, F. Tian, B. Adams-Huet, *et al.*, "Novel wavelet real time analysis of neurovascular coupling in neonatal encephalopathy," Sci. Rep. **7**(1), 45958 (2017).
11. A. M. Chiarelli, D. Perpetuini, P. Croce, *et al.*, "Evidence of neurovascular un-coupling in mild Alzheimer's disease through multimodal EEG-fNIRS and multivariate analysis of resting-state data," Biomedicines **9**(4), 337 (2021).
12. F. Al-Shargie, M. Kiguchi, N. Badruddin, *et al.*, "Mental stress assessment using simultaneous measurement of EEG and fNIRS," Biomed. Opt. Express **7**(10), 3882 (2016).
13. R. J. Deligani, S. B. Borgheai, J. McLinden, *et al.*, "Multimodal fusion of EEG-fNIRS: a mutual information-based hybrid classification framework," Biomed. Opt. Express **12**(3), 1635 (2021).
14. J. Uchitel, E. E. Vidal-Rosas, R. J. Cooper, *et al.*, "Wearable, integrated EEG-fNIRS technologies: a review," Sensors **21**(18), 6106 (2021).
15. S. Ahn and S. C. Jun, "Multi-modal integration of EEG-fNIRS for brain-computer interfaces – current limitations and future directions," Front. Hum. Neurosci. **11**, 503 (2017).
16. M. B. First, "Diagnostic and Statistical Manual of Mental Disorders, 5th Edition, and Clinical Utility," Journal of Nervous & Mental Disease **201**(9), 727–729 (2013).
17. M. Xia, J. Wang, and Y. He, "BrainNet viewer: a network visualization tool for human brain connectomics," PLoS One **8**(7), e68910 (2013).
18. A. Delorme and S. Makeig, "EEGLAB: an open source toolbox for analysis of single-trial EEG dynamics including independent component analysis," J. Neurosci. Methods **134**(1), 9–21 (2004).
19. A. Villringer and B. Chance, "Non-invasive optical spectroscopy and imaging of human brain function," Trends Neurosci. **20**(10), 435–442 (1997).

Biomedical Optics EXPRESS

20. F. A. Fishburn, R. S. Ludlum, C. J. Vaidya, *et al.*, "Temporal derivative distribution repair (TDDR): A motion correction method for fNIRS," NeuroImage **184**, 171–179 (2019).
21. M. A. Franceschini, S. Fantini, J. H. Thompson, *et al.*, "Hemodynamic evoked response of the sensorimotor cortex measured noninvasively with near-infrared optical imaging," Psychophysiology **40**, 548–560 (2003).
22. X. Hou, Z. Zhang, C. Zhao, *et al.*, "NIRS-KIT: a MATLAB toolbox for both resting-state and task fNIRS data analysis," Neurophotonics **8**(01), 010802 (2021).
23. R. D. Pascual-Marqui, C. M. Michel, and D. Lehmann, "Low resolution electromagnetic tomography: a new method for localizing electrical activity in the brain," International Journal of Psychophysiology **18**(1), 49–65 (1994).
24. R. D. Pascual-Marqui, "Coherence and phase synchronization: generalization to pairs of multivariate time series, and removal of zero-lag contributions," (2007).
25. J. Wang, X. Wang, M. Xia, *et al.*, "GRETNA: a graph theoretical network analysis toolbox for imaging connectomics," Front. Hum. Neurosci. **9**, 00386 (2015).
26. S. Tak, K. E. Jang, J. Jung, *et al.*, "NIRS-SPM: statistical parametric mapping for near infrared spectroscopy," in *Biomedical Optics (BiOS) 2008*, F. S. Azar and X. Intes, eds. (2008), p. 68500T.
27. F. Musso, J. Brinkmeyer, A. Mobascher, *et al.*, "Spontaneous brain activity and EEG microstates. A novel EEG/fMRI analysis approach to explore resting-state networks," NeuroImage **52**(4), 1149 (2010).
28. H. Yuan, V. Zotev, R. Phillips, *et al.*, "Spatiotemporal dynamics of the brain at rest — Exploring EEG microstates as electrophysiological signatures of BOLD resting state networks," NeuroImage **60**(4), 2062–2072 (2012).
29. B. T. Thomas Yeo, F. M. Krienen, J. Sepulcre, *et al.*, "The organization of the human cerebral cortex estimated by intrinsic functional connectivity," J. Neurophysiol. **106**(3), 1125–1165 (2011).
30. E. Hancer, B. Xue, and M. Zhang, "Differential evolution for filter feature selection based on information theory and feature ranking," Knowledge-Based Systems **140**, 103–119 (2018).
31. K. Park, W. Chen, N. D. Volkow, *et al.*, "Hemodynamic and neuronal responses to cocaine differ in awake versus anesthetized animals: Optical brain imaging study," NeuroImage **188**, 188–197 (2019).
32. J. Petrovic, V. Milosevic, M. Zivkovic, *et al.*, "Slower EEG alpha generation, synchronization and "flow"-possible biomarkers of cognitive impairment and neuropathology of minor stroke," PeerJ **5**, e3839 (2017).
33. N. Hofle, T. Paus, D. Reutens, *et al.*, "Regional cerebral blood flow changes as a function of delta and spindle activity during slow wave sleep in humans," J. Neurosci. **17**(12), 4800–4808 (1997).
34. M. Koskinen, T. Seppänen, J. Tuukkanen, *et al.*, "Propofol anesthesia induces phase synchronization changes in EEG," Clin. Neurophysiol. **112**(2), 386–392 (2001).
35. M. Malekmohammadi, N. AuYong, C. M. Price, *et al.*, "Propofol-induced changes in α-β sensorimotor cortical connectivity," Anesthesiology **128**(2), 305–316 (2018).
36. H. Gu, B. J. Salmeron, T. J. Ross, *et al.*, "Mesocorticolimbic circuits are impaired in chronic cocaine users as demonstrated by resting-state functional connectivity," NeuroImage **53**(2), 593–601 (2010).
37. N. Ma, Y. Liu, X.-M. Fu, *et al.*, "Abnormal brain default-mode network functional connectivity in drug addicts," PLoS One **6**(1), e16560 (2011).
38. H. Khajehpour, B. Makkiabadi, H. Ekhtiari, *et al.*, "Disrupted resting-state brain functional network in methamphetamine abusers: A brain source space study by EEG," PLoS One **14**(12), e0226249 (2019).
39. L. Degenhardt, F. Charlson, A. Ferrari, *et al.*, "The global burden of disease attributable to alcohol and drug use in 195 countries and territories, 1990–2016: a systematic analysis for the Global Burden of Disease Study 2016," The Lancet Psychiatry **5**(12), 987–1012 (2018).